Experimental assessment of the practical oxidative stability of lithium thiophosphate solid electrolytes

Georg F. Dewald[a,b], Saneyuki Ohno[a,b], Marvin A. Kraft[a,b], Raimund Koerver[a,b], Paul Till[a,b], Nella M. Vargas-Barbosa[c*], Jürgen Janek[a,b*], Wolfgang G. Zeier[a,b*]

[a]*Institute of Physical Chemistry, Justus-Liebig-University Giessen, Heinrich-Buff-Ring 17, D-35392 Giessen, Germany.*

[b]*Center for Materials Research (LaMa), Justus-Liebig-University Giessen, Heinrich-Buff-Ring 16, D-35392 Giessen, Germany.*

[c]*Max Planck Institute for Solid State Research, Heisenbergstrasse 1, 70569 Stuttgart Germany*

Abstract

All-solid-state batteries are often expected to replace conventional lithium-ion batteries in the future. However, the practical electrochemical and cycling stability of the best-conducting solid electrolytes, i.e. lithium thiophosphates, are still critical issues that prevent long-term stable high-energy cells. In this study, we apply a *stepwise cyclic voltammetry* approach to obtain information on the practical oxidative stability limit of $Li_{10}GeP_2S_{12}$, two different Li_2S-P_2S_5 glasses, as well as the argyrodite Li_6PS_5Cl solid electrolytes. We employ indium metal and carbon black as the counter and working electrodes, respectively, the latter to increase the interfacial contact area to the electrolyte as compared to the commonly used planar steel electrodes. Using a stepwise increase in the reversal potentials, the onset potential of oxidative decomposition at the electrode-electrolyte interface at 25 °C is identified. X-ray photoelectron spectroscopy is used to investigate the oxidation of sulfur(-II) in the thiophosphate polyanions to sulfur(0) as the dominant redox process in all electrolytes tested. Our results suggest that – in later cycles – the crystalline solid electrolyte itself is not the major redox active phase, but rather that only after the formation of such electrolyte decomposition products, significant redox behavior is observed. Indeed, the redox behavior of the decomposition products is an additional contributor to the overall cell capacity of solid-state batteries. The *stepwise cyclic voltammetry* approach presented here shows that the practical oxidative stability at 25 °C of thiophosphate solid electrolytes against carbon is kinetically higher than predicted by thermodynamic calculations, and that the decomposition

products dominate the redox behavior of cathode composites. The method serves as an efficient guideline for the determination of practical, kinetic stability limits of solid electrolytes with respect to the employed electrode materials.

1. Introduction.

As lithium-ion batteries are soon expected to reach their physical performance limits,[1] all-solid-state lithium batteries (SSBs) are currently investigated as an alternative approach to achieve high-energy cells. By replacing liquid electrolytes with solid electrolytes (SEs), the lithium metal anode and high-voltage cathode materials may be accessible, leading to a higher volumetric energy density. Among the large variety of SEs, the lithium thiophosphates are seen as promising candidates due to their high conductivity and processability at room temperature.[2–4]

Similar to lithium-ion batteries, in SSBs, the often-evolving interfaces and interphases control the performance and stability. A parameter that encompasses such interfaces and the formation of such interphases is the electrochemical stability window of the electrolyte. The electrochemical stability window (or simply electrochemical window, EW) is the potential range in which the electrolyte and its components are non-reactive, *i.e.* exhibits inertness towards oxidation and reduction. We note that the inertness depends strongly on the composition of the electrolyte itself as well as the electrode materials used. Recent theoretical calculations predict a small EW for thiophosphate electrolyte/electrode interfaces, which are limited by sulfur redox reactions at the cathode and by phosphorous redox reactions at the anode.[5–8]

Experimentally, the EW of SE is usually probed via cyclic voltammetry (CV).[6,9–11] Commonly, an asymmetric cell setup with lithium metal (acting as both counter and reference electrode) and a planar inert blocking electrode (as working electrode, usually planar stainless steel but sputtered gold and Pt are also reported) is used.[12–14] Once assembled, the cell is cycled at a fixed scan rate, often starting at the open-circuit potential, up to a certain positive potential (reported values range from 5 – 10 V vs. Li^+/Li) back to ca. 0 V vs. Li^+/Li and the cycle ends at the open-circuit voltage. The EW is established by arbitrarily choosing a cut-off current density, e.g. ± 1 mA/cm^2, for the upper and lower potential limits of the EW. Han *et al.*[6] recently showed that working electrodes with higher surface areas in contact with thiophosphate SEs show a lower onset potential of decomposition reactions and, therefore, a smaller EW. It is important to recall that the Faradaic current for any electrochemical reaction is proportional to the area of the electrode, the

concentration and diffusion coefficient of redox active species, and the number of electrons transferred. The surface area increase of the working electrode and the subsequent reduction of the EW is, therefore, somewhat expected since the increased contact area at the thiophosphate electrolyte/working electrode interface allows one to probe more of this interface. Even so, the EW reported by Han *et al.* is not only significantly smaller than other reports on similar materials, but also closely matches what is theoretically predicted. As such, until now, it has been presumed that thiophosphate-based SEs are not stable enough for SSBs and that the measured capacities of SSBs that contain these electrolytes are strongly affected by the redox activity of the SE itself. Although decomposition reactions have been reported in the cathode composites in SSBs,[7,8,12,15–22] their precise onset potentials and influence on the EW of SEs remains unclear.[18]

Benck *et al.*[19] developed a CV experiment with a progressively extended potential range to probe the EW of different conducting substrates in aqueous electrolytes. This methodology helps on associating oxidation and reduction features with corresponding coupled processes. Using this approach, in this work, we apply a stepwise cyclic voltammetry approach to determine the onset potential of oxidative electrolyte decomposition against carbon black and further study the electrochemical behavior after oxidative decomposition. More specifically, stepwise cyclic voltammetry in combination with X-ray photoelectron spectroscopy (XPS) is used to deduce the practical, kinetic stability limit against oxidation of $Li_{10}GeP_2S_{12}$, 70:30 as well as a 75:25 Li_2S-P_2S_5 glass, and Li_6PS_5Cl, all of which are discussed as potential SEs for SSBs. For our model study, we replace the inert blocking electrode with a SE-carbon black composite electrode that increases the interfacial contact between the components, and thus, the sensitivity of the measurement, similar to Han *et al.*[6] Since electronically conducting additives are frequently used in solid state composite cathodes and their implementation is a necessity for electronically and ionically isolating active materials, e.g. in Li-S batteries,[15,20–22] this setup can be employed to determine the practical EWs for application in the development of Li-S solid state batteries. As the electrolytes are expected to decompose in contact with Li metal,[23–26] indium metal is used as counter electrode to minimize the reaction current arising from the decomposition on the anode side, as demonstrated recently by Wagemaker *et al*.[27]

Although the redox activity of the SEs, i.e. $Li_{10}GeP_2S_{12}$, Li_3PS_4, Li_2S-P_2S_5 glasses and Li_6PS_5Cl at positive potentials has been recently reported,[18,28–32] we hope to shed further light into the

decomposition behavior of those materials. Indeed, our results show that the redox activity of these materials is not due to the crystalline SE itself, but rather due to the side-products formed upon electrolyte decomposition in early cycles. Therefore, in contrast to the current understanding that the structural electrolyte itself is redox active, this work suggests that only after the decomposition has occurred, the electrolytes' decomposition products dominate the redox activity in the CV scans, which can easily be misinterpreted as the EW in non-stepwise CV scans to high potentials.[6,33] Further, we report that the upper potential limit of the tested electrolytes against oxidation is significantly higher than theoretically predicted,[6] namely ca. 0.5 V – 1 V higher than thermodynamically predicted. This implies that the decomposition products of the solid electrolytes typically show much lower overvoltages in their redox behavior. Unfortunately, the stability range remains narrower than the cyclization limit of typical oxide-based cathode active materials. As such, our results make a strong case for the further development of protective oxide coatings that prevent interfacial decomposition at the electrolyte-cathode interface.[3,34] Additionally, as recently shown by Yu *et al.*[27] and Tan *et al.*[18], the reversible redox reactions of decomposition products contribute to the overall cell capacity in a SSB and cannot be neglected. The method and results presented here serve as a guideline for future SE benchmarking studies under practical conditions. Most valuable is the fact that the presented methodology can be used to fine-tune the limiting potentials during cyclization to achieve stable cycling of SSBs. In doing so, the performance of SSBs should increase when detrimental side-reactions due to electrolyte decomposition are avoided.

2. Experimental Methods.

Synthesis of solid electrolytes. The SEs as well as all related samples were handled only under argon atmosphere (O_2 < 1 ppm, H_2O < 5 ppm). For synthesis of electrolytes, a solid-state route was chosen. Lithium sulfide (Li_2S, Sigma Aldrich, 99.98 %), phosphorus pentasulfide (P_2S_5, Sigma Aldrich, 99 %), germanium sulfide (GeS, Sigma Aldrich, 99.99 %), anhydrous lithium chloride (LiCl, Alfa Aesar, 99%) and elemental sulfur (S_8, Arcos Organics, >99.999 %) were used as starting materials. For $Li_{10}GeP_2S_{12}$, the reactants were mixed in stoichiometric ratio in a 3 g batch. An excess of elemental sulfur (3 wt%) was added to compensate for evaporation losses. The

mixture was ball milled (Fritsch Pulverisette 7 premium line) in a ZrO_2 milling set (80 mL bowl and 90 g of milling balls with a diameter of 3 mm). The milling was conducted at 400 rpm in 150 cycles of each 15 min milling and 15 min cooling break. Subsequently, the powder was pressed into 10 mm diameter pellets and sealed under vacuum into a quartz ampoule. Heating was performed in a Nabertherm tube furnace for 20 h at 773 K (ramp 27 $K \cdot h^{-1}$) before homogenizing the sample in an agate mortar for 15 min.

To obtain the argyrodite Li_6PS_5Cl, the stoichiometric amount of the described precursors was mixed and ground for 15 min in an agate mortar. The mixture was pelletized and sealed under vacuum into an ampoule, followed by annealing at 823 K for 7 days (ramp 100 $K \cdot h^{-1}$) and subsequent grinding after the reaction was completed.

The Li_2S-P_2S_5 glasses was synthesized in 3 g batches by ball milling the starting materials (milling set up as described above) for 300 cycles of 5 min milling and 15 min break with 500 rpm.

Characterization of electrolytes. Phase purity was confirmed via X-ray diffraction (XRD). Measurements were performed on a PANalytical Empyrean powder diffractometer in Bragg-Brentano θ-θ geometry using Cu Kα radiation (λ_1 = 154.056 pm, λ_2 = 154.539 pm). A 2θ range of 10° to 90° was scanned in a step size of 0.026° (counting time per step 200 s). Samples were prepared on a (911)-oriented Si zero background holder and protected from ambient atmosphere by a Kapton® polyimide film. Diffractograms are shown in Figure S1 – S3.

For analysis of crystalline samples, Rietveld refinements were carried out employing the TOPAS-Academic V6 software package (Bruker). A 2θ range of 26−90° was refined using a Thompson-Cox-Hastings pseudo-Voigt function for the profile shape. The structural models published by Weber *et al.* and Kraft *et al.* were used as starting points for refinements.[35,36] Lithium parameters were taken from the respective neutron powder diffraction results and were not refined. For both samples, only minor side phases were found and the obtained structural information can be found in the Supporting Information.

To determine the conductivity of the SEs, 200 mg of the powder were pressed isostatically into 10 mm diameter pellets, contacted with around 200 nm of gold on each side with a diameter of 8.2 mm (deposited via thermal evaporation), and placed into pouch cells for impedance spectroscopy. Analysis was performed at 298 K using a VMP300 potentiostat (Biologic) in the frequency range between 7 MHz and 100 mHz with an amplitude of 10 mV. Taking the geometric

dimensions of the pellet into account, conductivities were calculated. Representative spectra are shown in Figure S4.

Preparation of carbon. Commercial carbon black with a BET-determined surface area of 62 $m^2 \cdot g^{-1}$ (Super C65, TIMCAL, Ltd.) was used as electronically conducting component of the working electrode composite. Here, two types of drying approaches were employed: (1) C65 dried in a Büchi oven under dynamic vacuum at a temperature of 300 °C for 24 h, and (2) C65 treated at 800 °C for 12 h under a reducing H_2/Ar flow (20 vol% H_2 in Ar).

Cyclic voltammetry (CV). For CV testing, press cells as previously described were used.[37] First, 60 mg of SE were filled into the PEEK housing and manually compressed with stainless steel stamps. For the SE-C electrode composite, SE and carbon were mixed in a weight ratio of 9:1 and manually ground in an agate mortar for 15 min. A mass of 12 mg of SE-C composite was put onto the SE pellet to prepare the working electrode (resulting in a theoretical thickness of around 160 µm for $Li_{10}GeP_2S_{12}$, calculated based on the components density). The sample was uniaxially pressed for 3 min at 35 kN. After adding 100 µm thick indium foil (ChemPur, 99.999 %) with a diameter of 9 mm as counter electrode on the other side of the pellet, the cell was fixed in an aluminum frame with a torque of 10 Nm, resulting in a pressure of approximately 60 MPa. Similar to the work by Wagemaker and coworkers,[27] indium metal was chosen as the counter and reference electrode material to ensure that no additional Li source is present for the experiments. Although only lithiated indium can be used as a reference electrode, a stable OCV of 0.62 V vs. Li^+/Li is established upon incorporation of ca. 1 at.% of Li in In.[38–40] As such, after assembly each cell was allowed to equilibrate for 1 h, to ensure good alloying at the counter/reference electrode and to establish a stable OCV prior to any measurements. Therefore, all data are reported against the potential of In/InLi. The stepwise CV experiments were performed using a VMP300 potentiostat (Biologic) at a constant temperature and scan rate of 298 K and 0.1 mV/s, respectively. Each experiment started at the open-circuit voltage (OCV), the potential was swept to the oxidative reversal potential, then back to 0.0 V vs. In/InLi, and the cycle finalized at the OCV. Two consecutive cycles were measured for each reversal potential studied. The following reversal potential ranges were measured: 1.6 to 3.2 V vs. In/InLi in 0.1 V step increases and from 3.2 to 4.4 V vs. In/InLi in 0.2 V steps. The instrumental resolution during CV experiments was 100 µV and 3 nA (accuracy 0.1 µA). In total, due to slow scan rate and the number of scans, a total step-wise CV experiment consumes about 35 days per sample.

The as-described cells (employing either vacuum dried or the surface-reduced C65) were also tested as full cells using chronopotentiometry at a current density of 200 $\mu A \cdot cm^{-2}$. In these cells, the $Li_{10}GeP_2S_{12}$ acted both as electrolyte and pseudo-active cathode material. Two different cells were tested up to two different cut-off potentials, 2 V and 3 V vs. In/InLi. The cells were initially charged to their respective cut-off potential and then discharged to 0 V vs. In/InLi.

X-ray photoelectron spectroscopy (XPS). For XPS measurements, a PHI Versaprobe II Scanning ESCA Microprobe (Physical Electronics PHI/ULVAC-PHI) with a monochromatized Al Kα X-ray source was used. Detailed spectra were recorded with a pass energy of the analyzer of 23.5 eV. Subsequently to disassembling the cell, the SE-C composite surface was investigated by XPS. Prior to recording, a representative surface area was selected by secondary electron imaging and the samples surface was cleaned for 5 min via Ar^+ sputtering (0.5 kV, 0.5 µA, area 36 mm^2). In addition to two reference samples of as-synthesized and as-mixed with carbon electrolytes, five samples were prepared for each electrolyte to investigate the influence of the applied potential. After the assembly of In/SE/SE-C cells, the potential was swept from OCV to 1 V, 2 V, 3 V, and 4 V vs. In/InLi with a rate 0.1 $mV \cdot s^{-1}$, respectively. The potential was kept constant at the set potential for 12 h to complete the reaction. One cell was kept at 4 V followed by 12 h at 0 V to check reversibility of the redox processes. Analysis was performed using the CasaXPS software package (Version 2.3.17). To calibrate the spectra to compensate for charging effects, the C 1s peak of pristine SE was assigned to aliphatic carbon and set to 284.8 eV. The resulting binding energy of the main intensity in S 2p detail spectrum was subsequently used to calibrate C65 containing samples.

3. Results.

Cyclic voltammetry. CV is a widely used method to investigate the stability of liquid electrolytes in order to corroborate their suitability for a wide range of applications.[19,41–43] Similar to liquid electrolytes, for SEs the experimental setup and the choice of electrode configuration, especially the lack of a true reference electrode, drastically influence the results obtained by CV, leading to a spread of information in the literature.[12–14,44–52] In solid-state materials, employing the commonly used planar stainless-steel electrodes for probing e.g. the decomposition reactions in $Li_{10}GeP_2S_{12}$ leads to small currents, even at a high potential of 5 V vs. In/InLi (see Figure 1, black trace), which suggests that this electrolyte is kinetically stable at these high potentials. However, due to sluggish kinetics in solids, the rate of decomposition will be limited to the solid/solid interface and the typical planar geometry with a small interface area leads to small currents. As the interfacial contact area between the SE and the electrode is increased upon the addition of carbon, Faradaic currents can be detected within the potential range in which the SE was previously seemingly stable (see Figure 1, red trace). Indeed, as presented in the introduction, Han *et al.*[6] recently showed this effect and concluded that the onset of decomposition does occur at lower potentials than when tested with planar electrodes, because more Faradaic features are evident in the measured CV.

Here, as C65 is used as the working electrode, the surface area of the blocking electrode is increased by roughly three orders of magnitude compared to the planar steel electrode. Considering typically currents measured during CV and the BET surface area of C65 (62 $m^2 \cdot g^{-1}$), the resulting current densities can be estimated to be in order of 10^{-5} $mA \cdot cm^{-2}$ (for 0.01 mA as shown in Figure 1). Due to the underlying microstructure, the true electrochemically active surface area remains unknown and normalization of the observed currents by the exact electrochemical surface area is not possible. However, planar electrodes are clearly not suitable for stability tests of SEs due to the small interfacial contact area in contrast to practical conditions in a solid-state battery. Such a planar measurement setup wrongly suggests a wide EW due to minor oxidation currents in the order of µA at high potentials. On the other hand, using the composite working electrode and measuring directly to high potentials leads to oxidation and reduction features in the CV that seem to be related to the stability of the measured electrolyte, but the precise onset of the decomposition remains unclear and, further, decomposition reactions cannot be distinguished from any subsequent redox-activity.

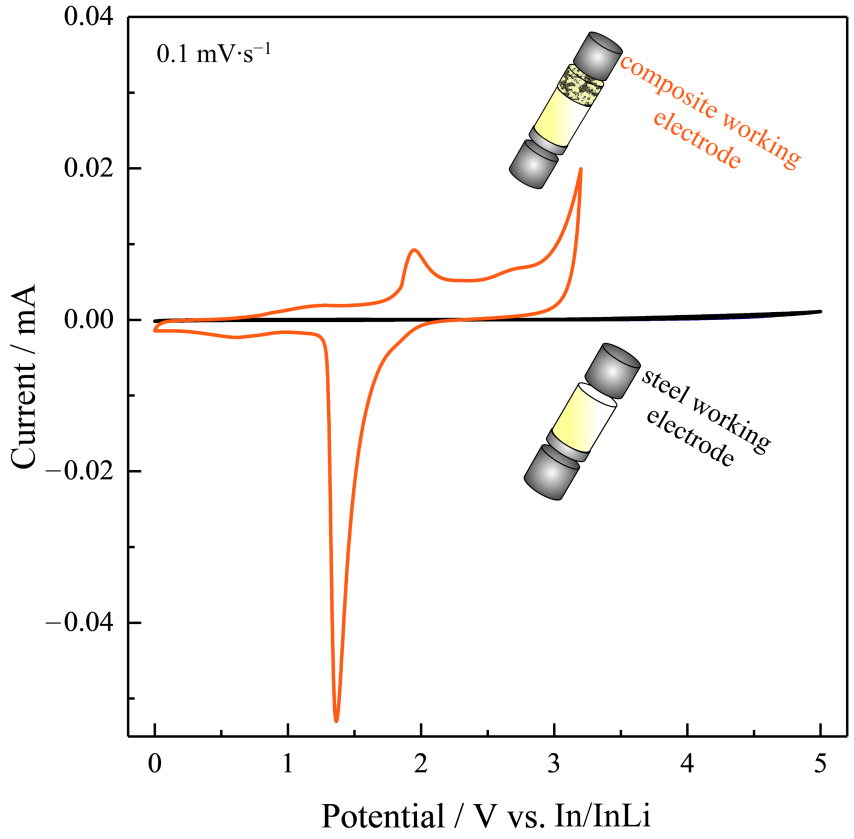

Figure 1: Visual comparison of two types of electrode morphology in CV experiments with the thiophosphate solid electrolyte $Li_{10}GeP_2S_{12}$. By employing In/InLi as both reference/counter electrode and planar stainless steel as working electrode, only small currents are detected (black). Adding a carbon-solid electrolyte composite electrode to the cell (orange) leads to higher currents and significant oxidative decomposition reactions are visible. The different currents are mainly due to the huge difference in interface area of the steel and carbon electrodes.

Stepwise cyclic voltammetry. In order to determine the onset potential of oxidative electrolyte decomposition, a careful stepwise approach of CV was employed to characterize $Li_{10}GeP_2S_{12}$, two Li_2S-P_2S_5 glasses (Li_2S:P_2S_5 ratio of 75:25 and 70:30) and Li_6PS_5Cl in asymmetrical cells. Each CV is measured twice up to a given reversal potential with a slow scan rate (0.1 mV·s^{-1}) followed by a stepwise increase of the potential range by 0.1 V up to 3.2 V vs. In/InLi and by 0.2 V from 3.4 V to 4.4 V vs. In/InLi. With this step-wise increase of the potential range, the reactivity of

decomposition products may be differentiated from any redox-activity of the pristine electrolyte (a schematic Figure of the experimental method is given in the Supporting Information, Figure S5). Figure 2 shows the resulting CV curves for experiments on $Li_{10}GeP_2S_{12}$. Full scans for the Li_2S-P_2S_5 glasses and the argyrodite Li_6PS_5Cl can be found in the Supporting Information (Figure S6 – S9). These measurements are taken against vacuum dried C65 carbon. However, as industrial carbons often exhibit OH-groups on the surface due to unsaturated carbon bonding, all experiments were repeated with reduced C65. [53] The resulting CV scans are shown in the Supporting Information (Figure S11 – S14).

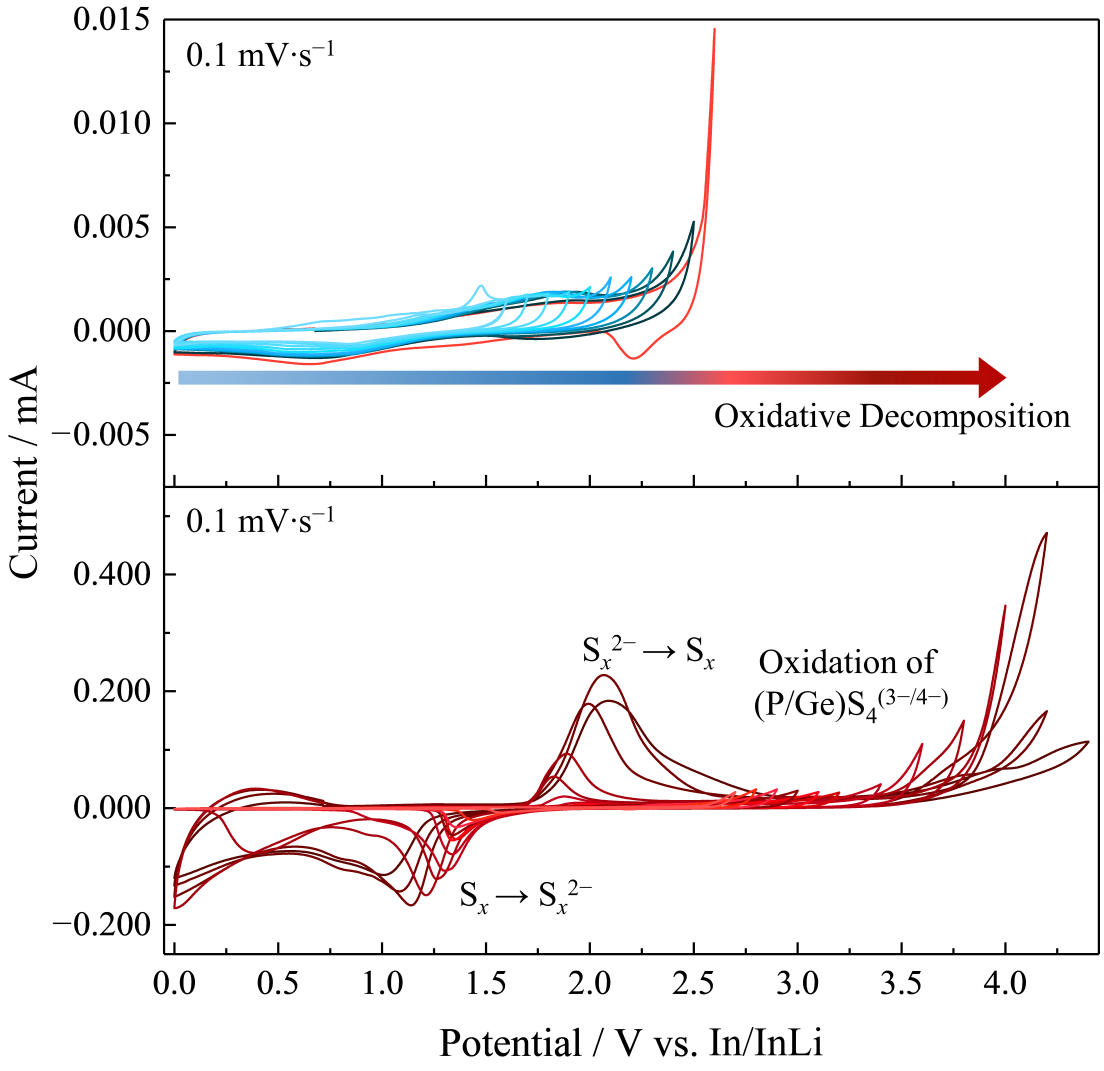

Figure 2: Stepwise cyclic voltammogram (0.1 mV·s^{-1}) for $Li_{10}GeP_2S_{12}$, using indium and a carbon-solid electrolyte composite as CE and WE, respectively. Up to 2.6 V, only minute currents are recorded (upper panel). Oxidative decomposition at high potentials (oxidation of $(P/GeS_4)^{(3-/4-)}$) leads to evolving peaks with varying peak area at potentials at which the SE was stable when lower reversal potentials were applied (lower panel). The latter processes are attributed to the redox activity of decomposed species ($S_x^{2-} \rightarrow S_x$) based on their corresponding peak potentials. Open-circuit voltage was 0.5 V vs. In/InLi. For clarity, only the first cycle at representative reversal potentials is shown. The full set of CVs can be found in the Supporting Information.

Figure 2 visually suggests that below a certain reversal potential (< 2.6 V vs. In/InLi) only minor, mostly capacitive currents on the order of µA are measured (current densities of about 10^{-6} mA·cm^{-2} with respect to the surface area of carbon working electrode). With increasing reversal potential, a significant increase in the maximum currents at the reversal potential (Figure S10) and additional anodic as well as cathodic peaks start to evolve. These new features occur within the previously stable range, suggesting that decomposition reactions are occurring at the composite electrode-electrolyte interface. Based on their peak potentials, these features are due to subsequent redox behavior of sulfur that stems from the decomposition of the $(P/Ge)S_4$ tetrahedral units, as further corroborated by X-ray photoemission spectroscopy (*vide infra*). In other words, the oxidation of the $(P/Ge)S_4$ tetrahedral units likely leads to elemental sulfur or polysulfides as well as other oxidized species such as the pyro-thiophosphate.[22] While back-reactions to the ortho-thiophosphate units are possible, the sulfur and/or polysulfides, likely both due to the broad potential range,[54] subsequently become redox-active. The observed changes in peak areas and peak potentials indicate changes in ohmic drop and the formation of resistive decomposed products.

Commonly, the stability window is defined by comparing CV experiments and choosing a current density or charge as cut-off criterion.[6,43,55] However, it needs to be emphasized that the resulting CV will strongly depend on the sample preparation, mixing of the composites, surface area of the carbon, and the experimental procedure. Hence, any selection of a current density cut-off is arbitrary. As an example, for $Li_{10}GeP_2S_{12}$, the first reduction peak occurs in the scan up to a reversal potential 2.6 V vs. In/LiIn with a peak current of 1.3 µA. The peak current is clearly distinguishable from previous scans and can therefore be attributed to a reduction reaction taking place. Therefore, to be consistent with the underlying chemistry, in this work, we define the

oxidative stability potential of the electrolyte at the reversal potential in which the CV does not show redox behavior (peaks) of the decomposition products in the following cycle. Hence, the uncertainty of this potential value is in the order of the step size used for the experiments (0.1 V). Based on this definition, $Li_{10}GeP_2S_{12}$ and Li_6PS_5Cl show similar stabilities with decomposition observed for potentials ≥ 2.6 V vs. In/InLi and ≥ 2.5 V vs. In/InLi, respectively. Despite the fact that two differently coordinated sulfur positions are present in Li_6PS_5Cl (PS_4^{3-} and "free" S^{2-}),[36] no significant difference between their stabilities was found within the experimental uncertainty. However, both glassy electrolytes of compositions 70:30 and 75:25 Li_2S-P_2S_5 show an lower oxidative stability limit of 2.2 V and 2.3 V vs. In/InLi, respectively. While 75:25 glass can be predominantly described by ortho-thiophosphate (PS_4^{3-}), with only minor contributions of pyro-thiodiphosphate ($P_2S_7^{4-}$), the 70:30 material contains both polyhedral species in a ratio of 1:1.[56,57] Although assigned with different local structural units, both glassy electrolytes show a comparable onset of oxidative decomposition and the reason for the observed lower stability of these SEs compared to the crystalline materials investigated in this study remains unclear. The oxidative (kinetic) stability limits of all electrolytes found here exceed the reported theoretical (thermodynamic) values[5,6] and they are significantly lower than previous experimental results obtained using a Li/SE/planar electrode setup.[11,14,48]

In comparison to the vacuum-dried carbon, a slight shift in the onset of oxidative decomposition on the order of 0.1 to 0.2 V was found for the stepwise CV and maximum currents for the reduced C65 (see Figure S11 – S15). In addition, higher currents can be detected in the CVs suggesting a better interfacial transfer kinetics with cleaner surfaces. However, considering the uncertainty of the measurement, no significant influence of surface treatment on the onset of oxidative decomposition can be established.

X-ray photoemission spectroscopy. Given the reported thiophosphate chemistry for β-Li_3PS_4,[29] oxidative decomposition of (P/Ge)S_4 tetrahedral building units in $Li_{10}GeP_2S_{12}$ is likely and may lead to the oxidation of S^{2-} to produce elemental sulfur or polysulfide species. Indeed, based on thermodynamic calculations, GeS_2, S_x, P_2S_5 and β-Li_3PS_4 (which in itself is unstable under oxidizing conditions) may all be expected as decomposition products of $Li_{10}GeP_2S_{12}$.[5,6,8] While the formation of crystalline P_2S_5 appears to be unlikely due to entropic reasons, the local formation of bridging sulfur, *i.e.* P-S_x-P bonds, likely takes place.[56] Highly resistive decomposition products

are expected to degrade the overall battery performance, which may explain the evolving overpotential and changing peak shape and potentials in the CV.[58] Interestingly, the formation of redox-active decomposition products such as elemental sulfur or polysulfide species may be the reason for the reduction peaks at lower potentials (2.5 − 1.5 V) as shown in Figure 2. After oxidative decomposition, a partially reversible reduction and oxidation behavior can be seen by the decomposition products as recently shown to influence the performance of SSBs.[29]

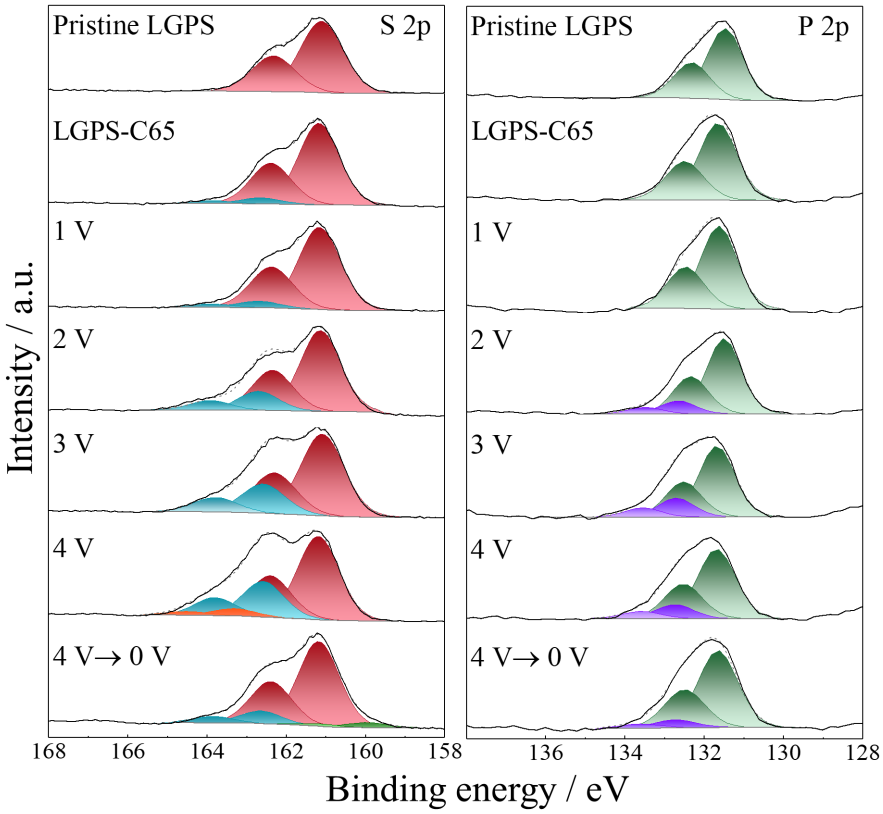

Figure 3: XPS characterization of $Li_{10}GeP_2S_{12}$-carbon composite. Shown are S 2p and P 2p signals. Treatment at 2V, 3 V respectively 4 V leads to a significant broadening and shift towards higher binding energies, indicating oxidation. Besides the main signal representing P-S bonds in PS_4^{3-} (shown in red respectively olive), a less intense signal, attributed to P-$[S]_n$-P bonds, was found in these oxidized samples. The oxidized species shown with orange peaks at 163.4 eV are reduced to be S^{2-} after the treatment at 0 V (green). All potentials are given relative to the In/InLi electrode.

To corroborate the presence and chemical nature of the decomposition products, the electrolyte-carbon composites were investigated using X-ray photoemission spectroscopy after applying a constant potential of 1 V, 2 V, 3 V, and 4 V vs. In/InLi for 12 h (see Figure 3 for $Li_{10}GeP_2S_{12}$). In addition, after 12 h of oxidation at 4 V vs. In/InLi, one sample was subsequently subject to a reduction potential of 0 V vs. In/InLi for 12 h. The XPS results are consistent with those obtained by CV. The phosphorus as well as germanium signal in the pristine $Li_{10}GeP_2S_{12}$ can be fitted with one species each as expected from the structure (Figure S16).[24,59] In addition to the expected terminal (P/Ge)-S bonding, a less intense second contribution at slightly higher binding energy can be identified in the S 2p spectra of the uncycled composites, which has been described before,[60] and is possibly related to the interaction between carbon surface or surface contaminants and SE.[54,61,62] While minor oxidative changes can be found in the sulfur binding energy for the untreated composite and at a potential of 1 V, only after treatment at 2 V and 3 V, respectively, significant shift towards higher binding energies can be found for both the sulfur and phosphorus signals. Here, an additional contribution starts to evolve in the S 2p and P 2p spectra at higher binding energies. As recently found, this oxidized species contains P-S_x-P bonds.[29,56] An evolving doublet at 163 eV that can be found in the S 2p spectrum of the composite treated at 4 V, which may be attributed to elemental sulfur.[15,29,63] These data collected on $Li_{10}GeP_2S_{12}$ (as well as Li_2S-P_2S_5 glasses and Li_6PS_5Cl, see Supporting Information) show that there is an onset of oxidative decomposition of the thiophosphate building units. For β-Li_3PS_4, polymerization of PS_4^{3-} units, leading to sulfur formation has been shown experimentally and proposed theoretically.[29,60,64,65] After oxidation at 4 V and subsequently applying 0 V vs. In/InLi, the oxidized species mostly disappear in the S 2p and P 2p spectra, further corroborating the redox-active nature of the decomposition products (P-S_x-P and S_x species) units as observed in the stepwise cyclic voltammetry. All three electrolytes show a reduced sulfur signal after applying a low potential (see also Figure S17 – S19), corroborating the reversal redox activity of elemental sulfur, while the decline of the oxidized P 2p signal indicates a fractional redox reaction of P-S_x-P type bonds. This is in line with previously reported X-ray photoemission results[22] that indicate the formation of P-S_x-P and S^0 species. One simplified oxidation exemplary reaction can be written as

$$2\ PS_4^{3-} \rightarrow P_2S_7^{4-} + S^0 + 2\ e^- . \quad (1)$$

However, given the variety of possible structural units in thiophosphate species, e.g. PS_4^{3-}, $P_2S_7^{4-}$, $P_2S_6^{2-}$ [29,56] the detailed oxidation pathway remains elusive. The specific binding state of sulfur is

uncertain, and we assume the formation of sulfur chains/rings of unknown length. Nevertheless, as P(+5) cannot be further oxidized, a linking of the ortho-thiophosphate PS_4^{3-} units towards $P_2S_7^{4-}$ or $P_2S_6^{2-}$ is expected and sulfur or polysulfide formation must occur.[22] While the oxidation of the local ortho-thiophosphate units to P-S-P (pyro-thiodiphosphates or meta-thiodiphosphates) is likely partially reversible due to the complex and coupled redox chemistry of thiophosphates,[27,66] a structural decomposition is not reversible and only the oxidized sulfur species that stem from the decomposition can be subsequently cycled reversibly as a redox active material.

Capacity evolution in solid-state batteries. The observed redox activity of the decomposition products may contribute the overall capacity and cell performance of a solid-state battery,[18,27,31,32] and the attainable capacities need to be monitored within and outside of the oxidative stability windows. In other words, it is important to establish if and how the redox activity of the decomposition products contributes additional charge to the overall system. As important is the correlation of the impedance increase due to the decomposition products with the redox activity.
In order to quantify this contribution, the described setup for the cyclic voltammetry was cycled with the C65-$Li_{10}GeP_2S_{12}$ composite acting as a cathode, without addition of an active material. As expected, when the cell is cycled within the kinetic oxidative stability window, only negligible charges (< 5 µAh, corresponding to $< 10^{-2}$ µAh·cm^{-2} with respect to the working electrode surface) are recorded (Figure 4a). However, with an upper cut-off potential of 3 V vs. In/InLi, which clearly lies outside of the stability window, charges on the order of 0.2 mAh are reversibly transferred (Figure 4b). Similar results and potential characteristics can be found using reduced carbon (see Figure S20), instead of vacuum-dried carbon, albeit with different capacities and slightly different overpotentials.
For a better comparison, the measurement result is further normalized to the mass of solid electrolyte in the cathode showing a significant influence of the decomposition reactions on the specific capacity when the electrolyte is decomposed. In a real SSB, i.e. with a known loading of a cathode active material, the contribution from the decomposition reactions will be higher because cathode active materials provide more active area for decomposition. In addition, as one would then normalize to the amount of known-active material but not the electrolyte itself, the additional specific capacitance may be significant. For instance, as a rough estimate, the total charge of

0.28 mAh obtained during the initial "charge" to 3 V vs. In/InLi correlates to 25 $mAh \cdot g_{SE}^{-1}$ for 10.8 mg of SE or to 105 $mAh \cdot g_{S}^{-1}$ for 2.66 mg of sulfur cathode active material in a typical loading for Li-S solid state batteries.[21] While conductive additives are vital for sulfur-based cathodes as the active material is electronically insulating, similar estimates can be made for NCM-based solid-state batteries. Indeed, while this estimate does not account for changes in contact areas, experimental conditions, changes in composite ratios and cathode processing, the decomposition products can lead to a significant capacity contribution in solid-state batteries. While it adds capacity to the battery operation, the resistive nature of the decomposition products (see above) will have detrimental implications on long-term cycling. Assuming the complete oxidation of $(P/Ge)S_4^{(3-/4-)}$ according to Equation (1), and with it the molar amounts of electrolyte decomposed based on measured charge of 0.28 mAh in the first scan, as well as the theoretical surface of carbon electrode material as an active reaction site, a reaction layer with a thickness of 13 nm can be expected (neglecting side reactions, changes in structure and density as well as assuming complete oxidation of $Li_{10}GeP_2S_{12}$, details on calculation are given in the Supporting Information).

These data underscore the non-trivial role of the thiophosphate electrolytes in solid-state batteries. While redox-activity in the SEs has been observed before,[28,29] these data show that the decomposition products clearly act as a pseudo-active material and thereby contribute to the overall cell performance, *i.e.* the cell capacity. Since the herein found oxidative stability limits lie inside the potential windows of typical cycling protocols, the capacity of the evolving interphase between SE, carbon and decomposition products cannot be neglected.

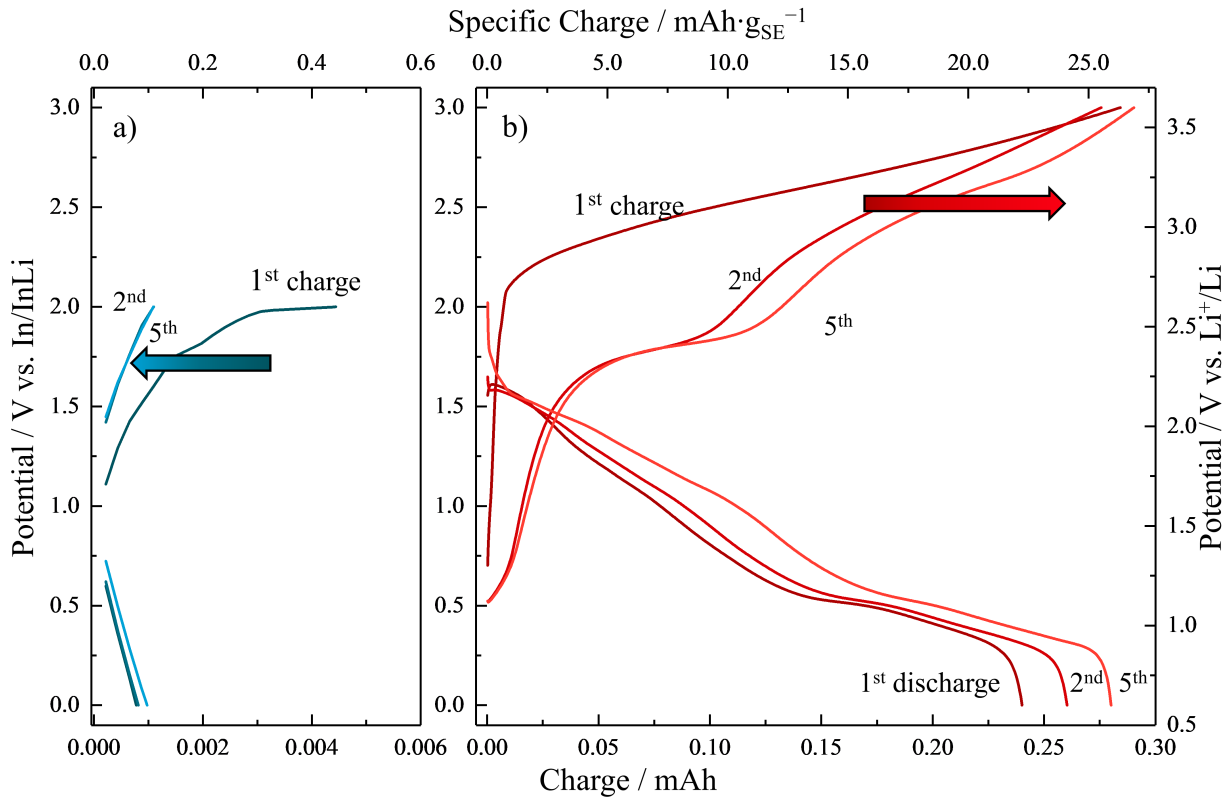

Figure 4: Charge-discharge curve of $Li_{10}GeP_2S_{12}$ acting as pseudo-active material in a composite cathode with carbon C65. While for cycling inside the stability window (≤ 2.0 V vs. In/InLi) only marginal charges are detected (a), a subsequently increasing capacity of 0.28 mAh is obtained in the first charge for an upper cut-off potential of 3 V vs. In/InLi and Li^+/Li (b). As the solid electrolyte acts as pseudo-active material, its contribution needs to be regarded in solid-state batteries, especially when a high-voltage cathode active material is employed. For calculation of the specific charge, the measured value is normalized to the mass of electrolyte (10.8 mg) in the cathode composite.

4. Discussion

The stepwise cyclic voltammetry performed here helps to determine the kinetic stability limit of solid electrolytes against oxidation, in this case for carbon C65 as electrode material. The experiments represent a model case study compared to a solid-state battery, as reactions with active materials are excluded. However, the results can be used to elucidate degradation mechanisms in carbon containing cells, and they may also be taken as hint for degradation at conventional NCM-based cathode materials. The upper stability limits against oxidation obtained here are shown in

Figure 5, together with recent theoretical predictions of stability windows.[5] The potentials of common cathode materials during cycling are also provided for reference. In this work, we have defined the detection of reduction peaks in the next cycle following an oxidative sweep as criterion for the stability limit against oxidation. Since the recorded current will strongly depend on sample preparation and experimental parameters, this comparative definition allows to define a practical stability limit using step-wise cyclic voltammetry. While it is trivial that an increasing surface area leads to higher currents and better resolved CVs, the stepwise CV provides the onset potentials of oxidative electrolyte decomposition. The solid electrolytes employed here show comparable potential limits for oxidation in the range between 2.2 V and 2.5 V vs. In/InLi (corresponding to 2.8 V and 3.1 V vs. Li^+/Li).[38] This shows that the experimental stability windows are wider than thermodynamically predicted. This is a reasonable result because the calculated stability represents the thermodynamic phase stability against competing phases at 0 K only, which excludes entropy contributions. In addition, the practical electrochemical stability windows obtained here must be viewed in relation to their respective cut-off criterion in which no redox activity of the decomposition reactions has been observed yet. Ongoing decomposition reactions may already take place as the X-ray photoemission spectra show small oxidative contributions on the surface already at lower potentials. However, as these cannot be seen in the CV yet, these windows reflect the practical stability window in which no influence on the cell performance is expected.

Although the electrochemically active area of the working electrode remains unknown, the results found herein represent practical oxidative stability limits, since the employed carbon is a frequently used additive. Taken together, the stepwise cyclic voltammetry and X-ray photoemission results show that the decomposition products become partially redox-active. We emphasize that while redox-activity of the building blocks of the electrolyte material itself is possible, *i.e.* linking and unlinking of thiophosphate units along with the production of sulfur, the consideration and detection of other redox active decomposition products is important. Ignoring the latter could lead to misinterpretation and would suggest significantly lower potential limits that hinder the viability of these SEs.[33] In other words, while a direct scan to high potentials (as shown in Figure 1) may suggest redox activity of the SE, the stepwise CV and X-ray photoemission spectra show that the redox activity largely comes from the decomposition products and that these decomposition products add significant capacity to the cell performance of a solid-state battery.

While the experimental results need to be referred to as a kinetic stability limit as opposed to thermodynamic stability, as they will strongly depend on the electrode material, its surface and microstructure as well as the applied current density in a cycling experiment, they can hint towards the practical oxidative stability limits of electrolytes. This means that for assessment of solid-state batteries, any stability window will have to be reestablished with the respective electrodes and carbons that are to be used. Since we have thoroughly analyzed the oxidative stability of these electrolytes, we can say that (1) the observed redox activity stems mostly from electrolyte decomposition products, which add capacity to all-solid-state battery cells, and (2) depending on the composition and transport properties of the occurring interphase, the decomposition layer will likely degrade the overall cell performance, as shown previously,[15,18,58,67] highlighting the need for the research and development of protective coatings in all-solid-state batteries.

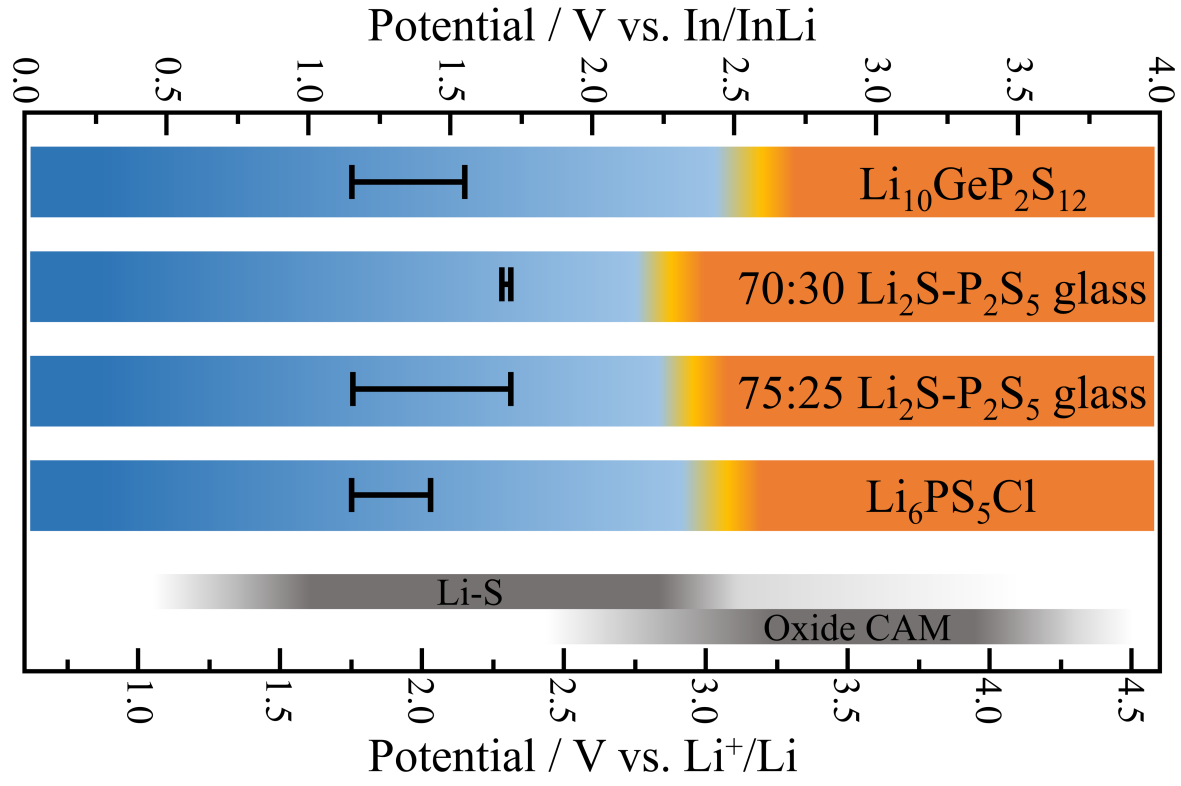

Figure 5: Practical oxidative stability limit of $Li_{10}GeP_2S_{12}$, Li_2S-P_2S_5 glasses and Li_6PS_5Cl against a carbon composite working electrode (indium metal counter electrode). The herein found stability region for each electrolyte is shown in blue and the onset of oxidative decomposition is shown in orange. Stability regions are derived from stepwise CV experiments from reversal potentials

without a recorded reduction peak. For comparison, theoretical results for thermodynamic stability ranges (black lines, taken from Zhu et al.[5]) and typical cycling windows of Li-S and oxide cathode active materials based cells are also shown. Note that the theoretical stability windows of the glassy Li_2S-P_2S_5 compounds refer to the corresponding crystalline phase $Li_7P_3S_{11}$ and β-Li_3PS_4.

Conclusion

In conclusion, the combination of stepwise cyclic voltammetry and X-ray photoemission shows the oxidative decomposition of $Li_{10}GeP_2S_{12}$, 70:30 as well as 75:25 Li_2S-P_2S_5 glass, and Li_6PS_5Cl electrolytes. In contrast to theoretical calculations, all electrolytes show a higher oxidative stability limit (between 2.2 V and 2.5 V vs. In/InLi, corresponding to 2.8 V and 3.1 V vs. Li^+/Li), when measured against carbon-containing composite working electrodes. Our work underscores the value of systematic and careful electrochemical experiments that employ high surface area electrodes to assess realistic stability windows of solid electrolytes for operation in battery cell configurations. It further shows that the practical oxidative stability limits are higher than the theoretically predicted (thermodynamic) values. Moreover, after electrolyte decomposition, the reaction products become redox-active and consequently contribute to the overall cell capacity in solid-state batteries.

This work shows that the careful stepwise cyclic voltammetry can address the practical, kinetic oxidative stability window of solid electrolytes and that these need to be measured anew once electrode compositions are changed. In general, improving the utilizable cycling window via composite or substitutional approaches may be possible. Further, coatings of electrode materials can then be designed to provide higher electrolyte stability in contact with the active cathode materials. By tailoring the electrolyte stability, long time cycling stability of solid-state batteries is expected to increase.

Associated Content

Supporting Information

The supporting information contains information on the synthesis and characterization (XRD, PEIS) of $Li_{10}GeP_2S_{12}$, Li_2S-P_2S_5 glass and Li_6PS_5Cl. Furthermore, additional CV data and a comparison of maximum currents at reversal potential during CV scans are enclosed. Also, XP detail spectra (S 2p, P 2p, Ge 3d) are provided for all solid electrolytes.

Corresponding Authors

*N.Vargas-Barbosa@fkf.mpg.de, *juergen.janek@pc.jlug.de, *wolfgang.g.zeier@pc.jlug.de;

Notes

The authors declare no competing financial interests.

Author contributions

N.M.V-B. and W.G.Z. designed the study and G.F.D. performed CV and SSB testing on $Li_{10}GeP_2S_{12}$ and Li_2S-P_2S_5 glasses and the fitting of XPS spectra. S.O. and M.A.K. performed CV testing on the Li_6PS_5Cl. G.F.D., S.O., and P.T. synthesized solid electrolytes. S.O. and R.K. performed XPS experiments. G.F.D., S.O., N.M.V-B., J.J., and W.G.Z. wrote the manuscript. All authors discussed the results and commented on the work.

Acknowledgements

The research was supported by the Federal Ministry of Education and Research (BMBF) within the project LISZUBA under grant number 03XP0115A. S.O. gratefully acknowledges the Alexander von Humboldt Foundation for partial financial support through a Postdoctoral Fellowship.

References

(1) Janek, J.; Zeier, W. G. A Solid Future for Battery Development. *Nat. Energy* **2016**, *1*, 16141.

(2) Jung, Y. S.; Oh, D. Y.; Nam, Y. J.; Park, K. H. Issues and Challenges for Bulk-Type All-Solid-State Rechargeable Lithium Batteries Using Sulfide Solid Electrolytes. *Isr. J. Chem.*

2015, *55*, 472–485.

(3) Culver, S. P.; Koerver, R.; Krauskopf, T.; Zeier, W. G. Designing Ionic Conductors: The Interplay between Structural Phenomena and Interfaces in Thiophosphate-Based Solid-State Batteries. *Chem. Mater.* **2018**, *30*, 4179–4192.

(4) Takada, K. Progress and Prospective of Solid-State Lithium Batteries. *Acta Mater.* **2013**, *61*, 759–770.

(5) Zhu, Y.; He, X.; Mo, Y. Origin of Outstanding Stability in the Lithium Solid Electrolyte Materials: Insights from Thermodynamic Analyses Based on First-Principles Calculations. *ACS Appl. Mater. Interfaces* **2015**, *7*, 23685–23693.

(6) Han, F.; Zhu, Y.; He, X.; Mo, Y.; Wang, C. Electrochemical Stability of $Li_{10}GeP_2S_{12}$ and $Li_7La_3Zr_2O_{12}$ Solid Electrolytes. *Adv. Energy Mater.* **2016**, *6*, 1501590.

(7) Zhu, Y.; He, X.; Mo, Y. First Principles Study on Electrochemical and Chemical Stability of Solid Electrolyte–Electrode Interfaces in All-Solid-State Li-Ion Batteries. *J. Mater. Chem. A* **2016**, *4*, 3253–3266.

(8) Lotsch, B. V.; Maier, J. Relevance of Solid Electrolytes for Lithium-Based Batteries: A Realistic View. *J. Electroceramics* **2017**, *38*, 128–141.

(9) Minami, K.; Hayashi, A.; Ujiie, S.; Tatsumisago, M. Electrical and Electrochemical Properties of Glass–Ceramic Electrolytes in the Systems Li_2S–P_2S_5–P_2S_3 and Li_2S–P_2S_5–P_2O_5. *Solid State Ionics* **2011**, *192*, 122–125.

(10) Liu, Z.; Fu, W.; Payzant, E. A.; Yu, X.; Wu, Z.; Dudney, N. J.; Kiggans, J.; Hong, K.; Rondinone, A. J.; Liang, C. Anomalous High Ionic Conductivity of Nanoporous β-Li_3PS_4. *J. Am. Chem. Soc.* **2013**, *135*, 975–978.

(11) Boulineau, S.; Courty, M.; Tarascon, J.-M.; Viallet, V. Mechanochemical Synthesis of Li-Argyrodite Li_6PS_5X (X = Cl, Br, I) as Sulfur-Based Solid Electrolytes for All Solid State Batteries Application. *Solid State Ionics* **2012**, *221*, 1–5.

(12) Richards, W. D.; Miara, L. J.; Wang, Y.; Kim, J. C.; Ceder, G. Interface Stability in Solid-State Batteries. *Chem. Mater.* **2016**, *28*, 266–273.

(13) Machida, N.; Yamamoto, H.; Asano, S.; Shigematsu, T. Preparation of Amorphous 75 $Li_2S \cdot x\ P_2S_3 \cdot (25\text{-}x)\ P_2S_5$ (mol%) Solid Electrolytes by a High-Energy Ball-Milling Process and Their Application for an All-Solid-State Lithium Battery. *Solid State Ionics* **2005**, *176*, 473–479.

(14) Kamaya, N.; Homma, K.; Yamakawa, Y.; Hirayama, M.; Kanno, R.; Yonemura, M.; Kamiyama, T.; Kato, Y.; Hama, S.; Kawamoto, K.; Mitsui, A. A Lithium Superionic Conductor. *Nat. Mater.* **2011**, *10*, 682–686.

(15) Zhang, W.; Leichtweiß, T.; Culver, S. P.; Koerver, R.; Das, D.; Weber, D. A.; Zeier, W. G.; Janek, J. The Detrimental Effects of Carbon Additives in $Li_{10}GeP_2S_{12}$-Based Solid-State Batteries. *ACS Appl. Mater. Interfaces* **2017**, *9*, 35888–35896.

(16) Park, K.; Yu, B. C.; Jung, J. W.; Li, Y.; Zhou, W.; Gao, H.; Son, S.; Goodenough, J. B. Electrochemical Nature of the Cathode Interface for a Solid-State Lithium-Ion Battery: Interface between $LiCoO_2$ and Garnet-$Li_7La_3Zr_2O_{12}$. *Chem. Mater.* **2016**, *28*, 8051–8059.

(17) Hänsel, C.; Afyon, S.; Rupp, J. L. M. Investigating the All-Solid-State Batteries Based on Lithium Garnets and a High Potential Cathode-$LiMn_{1.5}Ni_{0.5}O_4$. *Nanoscale* **2016**, *8*, 18412–18420.

(18) Tan, D. H. S.; Wu, E. A.; Nguyen, H.; Chen, Z.; Adam, M.; Marple, T.; Doux, J.-M.; Wang, X.; Yang, H.; Banerjee, A.; Meng, Y. S. Elucidating Reversible Electrochemical Redox of Li_6PS_5Cl Solid Electrolyte. *ACS Energy Lett.* **2019**.

(19) Benck, J. D.; Pinaud, B. A.; Gorlin, Y.; Jaramillo, T. F. Substrate Selection for Fundamental Studies of Electrocatalysts and Photoelectrodes: Inert Potential Windows in Acidic, Neutral, and Basic Electrolyte. *PLoS One* **2014**, *9*, e107942.

(20) Nagata, H.; Chikusa, Y. All-Solid-State Lithium-Sulfur Battery with High Energy and Power Densities at the Cell Level. *Energy Technol.* **2016**, *4*, 484–489.

(21) Ohno, S.; Koerver, R.; Dewald, G.; Rosenbach, C.; Titscher, P.; Steckermeier, D.; Kwade, A.; Janek, J.; Zeier, W. G. Observation of Chemomechanical Failure and the Influence of Cutoff Potentials in All-Solid-State Li–S Batteries. *Chem. Mater.* **2019**, *31*, 2930–2940.

(22) Mizuno, F.; Hayashi, A.; Tadanaga, K.; Tatsumisago, M. Design of Composite Positive Electrode in All-Solid-State Secondary Batteries with Li_2S-P_2S_5 Glass-Ceramic Electrolytes. *J. Power Sources* **2005**, *146*, 711–714.

(23) Wenzel, S.; Weber, D. A.; Leichtweiss, T.; Busche, M. R.; Sann, J.; Janek, J. Interphase Formation and Degradation of Charge Transfer Kinetics between a Lithium Metal Anode and Highly Crystalline $Li_7P_3S_{11}$ Solid Electrolyte. *Solid State Ionics* **2016**, *286*, 24–33.

(24) Wenzel, S.; Randau, S.; Leichtweiß, T.; Weber, D. A.; Sann, J.; Zeier, W. G.; Janek, J. Direct Observation of the Interfacial Instability of the Fast Ionic Conductor $Li_{10}GeP_2S_{12}$ at

the Lithium Metal Anode. *Chem. Mater.* **2016**, *28*, 2400–2407.

(25) Wenzel, S.; Sedlmaier, S. J.; Dietrich, C.; Zeier, W. G.; Janek, J. Interfacial Reactivity and Interphase Growth of Argyrodite Solid Electrolytes at Lithium Metal Electrodes. *Solid State Ionics* **2018**, *318*, 102–112.

(26) Hartmann, P.; Leichtweiss, T.; Busche, M. R.; Schneider, M.; Reich, M.; Sann, J.; Adelhelm, P.; Janek, J. Degradation of NASICON-Type Materials in Contact with Lithium Metal: Formation of Mixed Conducting Interphases (MCI) on Solid Electrolytes. *J. Phys. Chem. C* **2013**, *117*, 21064–21074.

(27) Yu, C.; Hageman, J.; Ganapathy, S.; van Eijck, L.; Zhang, L.; Adair, K.; Sun, X.; Wagemaker, M. Tailoring Li_6PS_5Br Ionic Conductivity and Understanding of Its Role in Cathode Mixtures for High Performance All-Solid-State Li-S Batteries. *J. Mater. Chem. A* **2019**, *7*, 10412–10421.

(28) Han, F.; Gao, T.; Zhu, Y.; Gaskell, K. J.; Wang, C. A Battery Made from a Single Material. *Adv. Mater.* **2015**, *27*, 3473–3483.

(29) Koerver, R.; Walther, F.; Aygün, I.; Sann, J.; Dietrich, C.; Zeier, W.; Janek, J. Redox-Active Cathode Interphases in Solid-State Batteries. *J. Mater. Chem. A* **2017**, *5*, 22750–22760.

(30) Auvergniot, J.; Cassel, A.; Foix, D.; Viallet, V.; Seznec, V.; Dedryvère, R. Redox Activity of Argyrodite Li_6PS_5Cl Electrolyte in All-Solid-State Li-Ion Battery: An XPS Study. *Solid State Ionics* **2017**, *300*, 78–85.

(31) Hakari, T.; Nagao, M.; Hayashi, A.; Tatsumisago, M. Preparation of Composite Electrode with Li_2S–P_2S_5 Glasses as Active Materials for All-Solid-State Lithium Secondary Batteries. *Solid State Ionics* **2014**, *262*, 147–150.

(32) Hakari, T.; Nagao, M.; Hayashi, A.; Tatsumisago, M. All-Solid-State Lithium Batteries with Li_3PS_4 Glass as Active Material. *J. Power Sources* **2015**, *293*, 721–725.

(33) Swamy, T.; Chen, X.; Chiang, Y.-M. Electrochemical Redox Behavior of Li Ion Conducting Sulfide Solid Electrolytes. *Chem. Mater.* **2019**, *31*, 707–713.

(34) Culver, S.; Koerver, R.; Zeier, W. G.; Janek, J. On the Functionality of Coatings for Cathode Active Materials in Thiophosphate-Based All-Solid-State Batteries. *Adv. Energy Mater.* **2019**, *9*, 1900626.

(35) Weber, D. A.; Senyshyn, A.; Weldert, K. S.; Wenzel, S.; Zhang, W.; Kaiser, R.; Berendts,

S.; Janek, J.; Zeier, W. G. Structural Insights and 3D Diffusion Pathways within the Lithium Superionic Conductor $Li_{10}GeP_2S_{12}$. *Chem. Mater.* **2016**, *28*, 5905–5915.

(36) Kraft, M. A.; Culver, S. P.; Calderon, M.; Böcher, F.; Krauskopf, T.; Senyshyn, A.; Dietrich, C.; Zevalkink, A.; Janek, J.; Zeier, W. G. Influence of Lattice Polarizability on the Ionic Conductivity in the Lithium Superionic Argyrodites Li_6PS_5X (X = Cl, Br, I). *J. Am. Chem. Soc.* **2017**, *139*, 10909–10918.

(37) Zhang, W.; Weber, D. A.; Weigand, H.; Arlt, T.; Manke, I.; Schröder, D.; Koerver, R.; Leichtweiss, T.; Hartmann, P.; Zeier, W. G.; Janek, J. Interfacial Processes and Influence of Composite Cathode Microstructure Controlling the Performance of All-Solid-State Lithium Batteries. *ACS Appl. Mater. Interfaces* **2017**, *9*, 17835–17845.

(38) Santhosha, A. L.; Medenbach, L.; Buchheim, J. R.; Adelhelm, P. The Indium-Lithium Electrode in Solid-State Lithium Ion Batteries: Phase Formation, Redox Potentials and Interface Stability. *Batter. Supercaps* **2019**, *2*, 524–529.

(39) Alexander, W. A.; Calvert, L. D.; Gamble, R. H.; Schinzel, K. The Lithium-Indium System. *Can. J. Chem.* **1976**, *57*, 1052–1060.

(40) Takada, K.; Aotani, N.; Iwamoto, K.; Kondo, S. Solid State Lithium Battery with Oxysulfide Glass. *Solid State Ionics* **1996**, *86–88*, 877–882.

(41) Xu, K. Nonaqueous Liquid Electrolytes for Lithium-Based Rechargeable Batteries. *Chem. Rev.* **2004**, *104*, 4303–4418.

(42) Aurbach, D.; Daroux, M.; Faguy, P. The Electrochemistry of Noble Metal Electrodes. *J. Electroanal. Chem* **1991**, *297*, 225–244.

(43) Campbell, S. A.; Bowes, C.; McMillan, R. S. The Electrochemical Behaviour of Tetrahydrofuran and Propylene Carbonate without Added Electrolyte. *J. Electroanal. Chem* **1990**, *284*, 195–204.

(44) Ue, M.; Ida, K.; Mori, S. Electrochemical Properties of Organic Liquid Electrolytes Based on Quaternary Onium Salts for Electrical Double-Layer Capacitors. *J. Electrochem. Soc.* **1994**, *141*, 2989–2996.

(45) Ward, K. R.; Compton, R. G. Quantifying the Apparent "Catalytic" Effect of Porous Electrode Surfaces. *J. Electroanal. Chem.* **2014**, *724*, 43–47.

(46) Sun, Y.; Suzuki, K.; Hara, K.; Hori, S.; Yano, T. A.; Hara, M.; Hirayama, M.; Kanno, R. Oxygen Substitution Effects in $Li_{10}GeP_2S_{12}$ solid Electrolyte. *J. Power Sources* **2016**, *324*,

798–803.

(47) Yu, C.; Eijck, L. Van; Ganapathy, S.; Wagemaker, M. Synthesis , Structure and Electrochemical Performance of the Argyrodite Li_6PS_5Cl Solid Electrolyte for Li-Ion Solid State Batteries. *Electrochim. Acta* **2016**, *215*, 93–99.

(48) Hayashi, A.; Kama, S.; Mizuno, F.; Tadanaga, K.; Minami, T.; Tatsumisago, M. Characterization of Li_2S-P_2S_5 Glass-Ceramics as a Solid Electrolyte for Lithium Secondary Batteries. *Solid State Ionics* **2004**, *175*, 683–686.

(49) Mutoro, E.; Luerßen, B.; Günther, S.; Janek, J. The Electrode Model System $Pt(O_2)$|YSZ: Influence of Impurities and Electrode Morphology on Cyclic Voltammograms. *Solid State Ionics* **2009**, *180*, 1019–1033.

(50) Xu, K.; Ding, S. P.; Richard Jow, T. Toward Reliable Values of Electrochemical Stability Limits for Electrolytes. *J. Electrochem. Soc.* **1999**, *146*, 4172–4178.

(51) Galiński, M.; Lewandowski, A.; Stepniak, I. Ionic Liquids as Electrolytes. *Electrochim. Acta* **2006**, *51*, 5567–5580.

(52) Bhide, A.; Hofmann, J.; Dürr, A. K.; Janek, J.; Adelhelm, P. Electrochemical Stability of Non-Aqueous Electrolytes for Sodium-Ion Batteries and Their Compatibility with Na0.7CoO2. *Phys. Chem. Chem. Phys.* **2014**, *16*, 1987–1998.

(53) Boehm, H. P. Some Aspects of the Surface Chemistry of Carbon Blacks and Other Carbons. *Carbon N. Y.* **1994**, *32*, 759–769.

(54) Medenbach, L.; Escher, I.; Köwitsch, N.; Armbrüster, M.; Zedler, L.; Dietzek, B.; Adelhelm, P. Sulfur Spillover on Carbon Materials and Possible Impacts on Metal-Sulfur Batteries. *Angew. Chemie Int. Ed.* **2018**, *57*, 13666–13670.

(55) Xu, K.; Ding, M. S.; Richard Jow, T. A Better Quantification of Electrochemical Stability Limits for Electrolytes in Double Layer Capacitors. *Electrochim. Acta* **2001**, *46*, 1823–1827.

(56) Dietrich, C.; Koerver, R.; Gaultois, M. W.; Kieslich, G.; Cibin, G.; Janek, J.; Zeier, W. G. Spectroscopic Characterization of Lithium Thiophosphates by XPS and XAS - a Model to Help Monitor Interfacial Reactions in All-Solid-State Batteries. *Phys. Chem. Chem. Phys.* **2018**, *20*, 20088–20095.

(57) Dietrich, C.; Weber, D.; Sedlmaier, S. J.; Indris, S.; Culver, S.; Walter, D.; Janek, J.; Zeier, W. Lithium Ion Conductivity in Li_2S-P_2S_5 Glasses – Building Units and Local

Structure Evolution during the Crystallization of the Superionic Conductors Li_3PS_4 , $Li_7P_3S_{11}$ and $Li_4P_2S_7$. *J. Mater. Chem. A* **2017**, *5*, 18111–18119.

(58) Koerver, R.; Aygün, I.; Leichtweiß, T.; Dietrich, C.; Zhang, W.; Binder, J. O.; Hartmann, P.; Zeier, W. G.; Janek, J. Capacity Fade in Solid-State Batteries: Interphase Formation and Chemomechanical Processes in Nickel-Rich Layered Oxide Cathodes and Lithium Thiophosphate Solid Electrolytes. *Chem. Mater.* **2017**, *29*, 5574–5582.

(59) Zhang, W.; Richter, F.; Culver, S. P.; Leichtweiß, T.; Lozano, J. G.; Dietrich, C.; Bruce, P. G.; Zeier, W. G.; Janek, J. Degradation Mechanisms at the $Li_{10}GeP_2S_{12}/LiCoO_2$ Cathode Interface in an All-Solid-State Lithium Ion Battery. *ACS Appl. Mater. Interfaces* **2018**, *10*, 22226–22236.

(60) Hakari, T.; Deguchi, M.; Mitsuhara, K.; Ohta, T.; Saito, K.; Orikasa, Y.; Uchimoto, Y.; Kowada, Y.; Hayashi, A.; Tatsumisago, M. Structural and Electronic-State Changes of a Sulfide Solid Electrolyte during the Li Deinsertion-Insertion Processes. *Chem. Mater.* **2017**, *29*, 4768–4774.

(61) Wang, J.; Chew, S. Y.; Zhao, Z. W.; Ashraf, S.; Wexler, D.; Chen, J.; Ng, S. H.; Chou, S. L.; Liu, H. K. Sulfur-Mesoporous Carbon Composites in Conjunction with a Novel Ionic Liquid Electrolyte for Lithium Rechargeable Batteries. *Carbon* **2008**, *46*, 229–235.

(62) Chin, H. C. Preparation and Characterization of Carbon-Sulfur Surface Compounds. *Carbon* **1981**, *19*, 175–186.

(63) Moulder, J. F.; Stickle, W. F.; Sobol, P. E.; Bomben, K. D. *Handbook of X-Ray Photoelectron Spectroscopy : A Reference Book of Standard Spectra for Identification and Interpretation of XPS Data*; Chastain, J., Ed.; Physical Electronics Division, Perkin-Elmer Corp, 1992.

(64) Sumita, M.; Tanaka, Y.; Ikeda, M.; Ohno, T. Charged and Discharged States of Cathode/Sulfide Electrolyte Interfaces in All-Solid-State Lithium Ion Batteries. *J. Phys. Chem. C* **2016**, *120*, 13332–13339.

(65) Sumita, M.; Tanaka, Y.; Ohno, T. Possible Polymerization of PS_4 at a Li_3PS_4 /$FePO_4$ Interface with Reduction of the $FePO_4$ Phase. *J. Phys. Chem. C* **2017**, *121*, 9698–9704.

(66) Ghidiu, M.; Ruhl, J.; Culver, S. P.; Zeier, W. G. Solution-Based Synthesis of Lithium Thiophosphate Superionic Conductors for Solid-State Batteries: A Chemistry Perspective. *J. Mater. Chem. A* **2019**, *7*, 17735–17753.

(67) Yoon, K.; Kim, J. J.; Seong, W. M.; Lee, M. H.; Kang, K. Author Correction: Investigation on the Interface between $Li_{10}GeP_2S_{12}$ electrolyte and Carbon Conductive Agents in All-Solid-State Lithium Battery. *Sci. Rep.* **2018**, *8*, 8066.

For table of contents only